ACS APPLIED MATERIALS & INTERFACES

Research Article

www.acsami.org

Effects of Number and Position of Meta and Para Carboxyphenyl Groups of Zinc Porphyrins in Dye-Sensitized Solar Cells: Structure–Performance Relationship

Ram B. Ambre, Sandeep B. Mane, Gao-Fong Chang, and Chen-Hsiung Hung*

Institute of Chemistry, Academia Sinica, Nankang, Taipei, 115 Taiwan

Supporting Information

ABSTRACT: Porphyrin sensitizers containing *meta*- and *para*-carboxyphenyl groups in their meso positions have been synthesized and investigated for their performance in dye-sensitized solar cells (DSSCs). The superior performance of para-derivative compared to meta-derivative porphyrins was revealed by optical spectroscopy, electrochemical property measurements, density functional theory (DFT) calculations, attenuated total reflectance-Fourier transform infrared (ATR-FTIR) spectroscopy, incident photon-to-current conversion efficiency (IPCE), electrochemical impedance spectroscopy (EIS), and stability performance. Absorption spectra of *para*-carboxyphenyl-substituted porphyrins on TiO_2 show a broader Soret band compared to *meta*-carboxyphenyl-substituted porphyrins. ATR-FTIR spectra of the studied porphyrins on TiO_2 were applied to investigate the number and mode of carboxyl groups attached to TiO_2. The V_{OC}, J_{SC}, and IPCE values of para-series porphyrins were distinctly superior to those of meta-series porphyrins. The Nyquist plots of the studied porphyrins show that charge injection in para-series porphyrins is superior to that in meta-series porphyrins. The orthogonally positioned para derivatives have more efficient charge injection and charge transfer over charge recombination, whereas the efficiencies of flat-oriented meta derivatives are retarded by rapid charge recombination. Photovoltaic measurements of the studied *meta*- and *para*-carboxyphenyl-functionalized porphyrins show that the number and position of carboxyphenyl groups play a crucial role in the performance of the DSSC. Our results indicate that *para*-carboxyphenyl derivatives outperform *meta*-carboxyphenyl derivatives to give better device performance. This study will serve as a guideline for the design and development of organic, porphyrin, and ruthenium dyes in DSSCs.

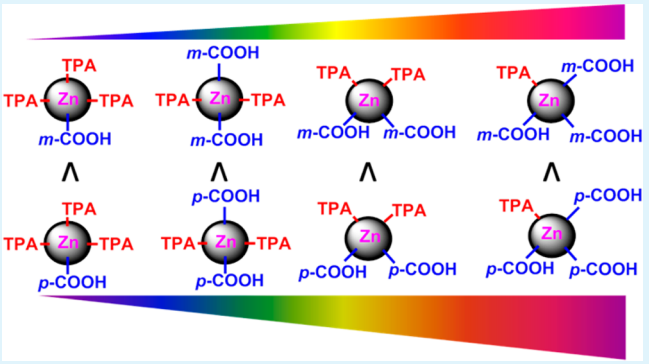

KEYWORDS: *dye-sensitized solar cells, metalloporphyrins, zinc porphyrin, sensitizers, dyes and pigments, dye orientation*

1. INTRODUCTION

Dye-sensitized solar cells (DSSCs) are emerging as important systems in the search for environmentally friendly and economically viable renewable energy sources.[1,2] These systems have offered diverse research golas, such as the design and synthesis of highly efficient sensitizing dyes, control of the morphology of TiO_2 photoanodes and platinum counter electrodes, the development of various electrolytes, and device fabrication techniques. Optimization in each of these areas has great importance in improving overall device efficiency. The design and synthesis of highly efficient sensitizers is the most attractive but challenging task. Several ruthenium, organic, and porphyrin dyes have been synthesized and investigated in terms of their performance in DSSCs.[3−7] Ruthenium dyes offer an average efficiency of 11%, but their application might be limited due to the scarcity of ruthenium metal and environmental concerns.[8−10] Organic dyes have attracted much attention because of their ease of synthesis and moderate efficiency, but ultrahigh efficiency and long-term stability have not yet been achieved.[11−13] The intrinsic rigid molecular structures, fast electron injection, and large absorption coefficients of porphyrins make them the most suitable candidates for use in DSSCs.[14−22] Moreover, the free internal core for metalation and four meso and eight β-pyrrole positions can be used for tuning their optical, electrochemical, and photophysical properties.[23−26] Currently, record high efficiencies of 12% and 13% were achieved by GY50 and SM315 porphyrin dyes, respectively, using a cobalt electrolyte under standard one-sun illumination.[27,28] It has been observed that the type of anchoring group attached to the semiconducting layer plays an important role in determining the power conversion efficiency and stability of dyes.[26,29] Carboxylic acid, carboxyphenyl groups, cyanoacrylic acid, phosphonic acid, sulfonic acid, carboxyl esters, and carboxyl salts have been studied as anchoring groups used in porphyrin sensitizers; however, the carboxyphenyl group is the most commonly used anchoring

Received: November 3, 2014
Accepted: January 6, 2015
Published: January 6, 2015

DOI: 10.1021/am507503d
ACS Appl. Mater. Interfaces 2015, 7, 1879−1891

unit in porphyrins for use in DSSCs. In the literature, very few articles have compared the effects of meta-anchoring versus para-anchoring units on the efficiency of DSSCs.[29−33] Campbell and co-workers reported that *meta*-carboxyphenyl-substituted porphyrins do not aggregate and lie flat on the TiO_2 conduction band (CB), which significantly increases the short-circuit current (I_{SC}) and and open-circuit voltage (V_{OC}) compared to those obtained using *para*-carboxyphenyl-substituted porphyrins.[5] Rochford et al. also reported that *meta*-carboxyphenyl porphyrin derivatives do not undergoes aggregation compared to *para*-carboxyphenyl porphyrin derivatives.[30] Odobel et al. showed that porphyrins containing *meta*-phenylphosphonic acids show superior cell performance compared to those containing *para*-phenylphosphonic acids.[29] Very recently, Si and He reported that *meta*- carboxyphenyl zinc porphyrin derivatives give lower performance than *para*-carboxyphenyl zinc porphyrin derivatives.[34] Figure 1 shows the

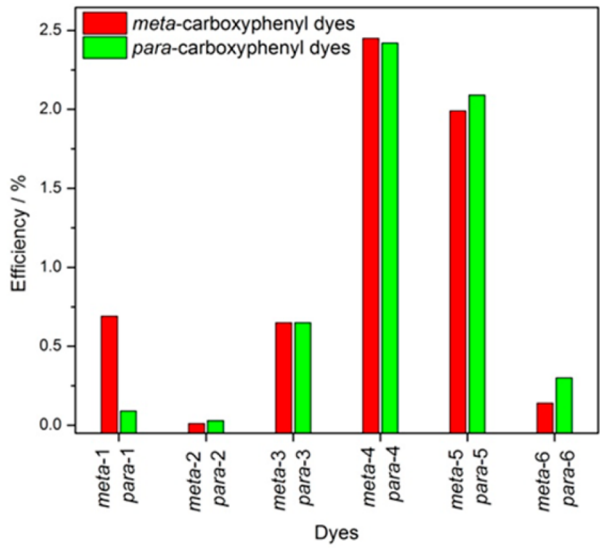

Figure 1. Efficiency comparison of meta-anchoring and para-anchoring dye derivatives. The names of the dyes in the respective article are included in parentheses. *meta*-1 (*m*-ZnTCPP-[S]),[30] *para*-1 (*p*-ZnTCPP-[S]),[30] *meta*-2 (10),[31] *para*-2 (9),[31] *meta*-3 (2p),[32] *para*-3 (2m),[32] *meta*-4 (2m-Zn),[32] *para*-4 (2m-Zn),[32] *meta*-5 (3m-Zn),[32] *para*-5 (3m-Zn),[32] *meta*-6 (4),[33] and *para*-6 (7).[33]

comparative efficiency data of meta- and para-anchoring units in porphyrins and organic dyes for use in DSSCs. Rochford et al. reported that the flat orientation of *meta*-$COOEt_3NH$-substituted porphyrin (*meta*-1 in Figure 1) gives greater charge injection into the TiO_2 CB, giving a higher efficiency and incident photon-to-current conversion efficiency (IPCE) than *para*-$COOEt_3NH$-substituted porphyrin (*para*-1 in Figure 1).[30] Lee et al. showed that *β*-substituted *para*-carboxyphenyl porphyrin (*para*-2 in Figure 1) gives a higher efficiency than *meta*-carboxyphenyl-substituted porphyrin (*meta*-2 in Figure 1).[31] Recently, a comparative DSSC performance study on *ortho*-carboxyphenyl-, *meta*-carboxyphenyl-, and *para*-carboxyphenyl-substituted porphyrin derivatives showed that the meta and para derivatives are distinctly superior to the ortho derivatives, although the meta derivatives (*meta*-3, *meta*-4, and *meta*-5 in Figure 1) and the para derivatives (*para*-3, *para*-4, and *para*-5 in Figure 1) give mixed performances.[32] In the case of azo organic dyes, *para*-carboxyphenyl-substituted dye (*para*-6 in Figure 1) gives a higher efficiency than *meta*-carboxyphenyl-substituted dye (*meta*-6 in Figure 1).[33]

Our laboratory has been focused on the development of novel regular porphyrins, core-modified porphyrins,[35,36] and expanded porphyrins[37] for DSSCs. To understand the effects of meso substituents on zinc porphyrins, we have designed series of porphyrins with various numbers and positions of *para*-carboxyphenyl and thienyl groups in the meso position and demonstrated that the performance of multianchoring porphyrins is distinctly superior to that of their monoanchoring porphyrin analogues.[38] Based on these fruitful conclusions, we have synthesized series of porphyrins with dual donor−acceptor units (2D-*π*-2A)[39] and porphyrins with three carboxyphenyl units (1D-*π*-3A).[40] The general trend observed for DSSC efficiency of the studied porphyrins was mono-carboxyphenyl- < *trans*-carboxyphenyl- < *cis*-carboxyphenyl- < tricarboxyphenyl-substituted porphyrins. After extracting these important conclusions from the above-mentioned studies, we became interested in studying the effects of meta- versus para-anchoring-group substitution on the efficiency of porphyrins in DSSCs. In this work, we have synthesized two series of porphyrins, classified as *meta*-carboxyphenyl-group-containing porphyrins, namely, Zn3TPA*m*1A, *trans*-Zn2TPA*m*2A, *cis*-Zn2TPA*m*2A, and Zn1TPA*m*3A, and *para*-carboxyphenyl-group-containing porphyrins, namely, Zn3TPA1A, *trans*-Zn2TPA2A, *cis*-Zn2TPA2A, and Zn1TPA3A. The molecular structures of meta- and para-series porphyrins are presented in Chart 1. In abbreviated names, Zn denotes the presence of zinc metal in the porphyrin core, TPA stands for the triphenylamine unit, and A stands for the carboxyphenyl unit. The numbers of TPA and carboxyphenyl units are denoted by the numerals preceding the corresponding abbreviations. The letter *m* is used to differentiate the meta position of the carboxyl unit of meta-series porphyrins. The prefixes cis and trans are used to indicate the position of the carboxyphenyl or TPA units.

2. RESULTS AND DISCUSSION

Synthesis. The synthetic procedures of the meta-series porphyrin sensitizers Zn3TPA*m*1A, *trans*-Zn2TPA*m*2A, *cis*-Zn2TPA*m*2A, and Zn1TPA*m*3A are presented in Scheme 1. Condensation of pyrrole, methyl 3-formylbenzoate, and 4-(diphenylamino)benzaldehyde catalyzed by boron trifluoride−diethyl etherate followed by subsequent oxidation by 2,3-dichloro-5,6-dicyano-*p*-benzoquinone (DDQ) afforded mixture of six porphyrins. The required porphyrins were separated by column chromatography, and subsequent metalation was readily achieved by reacting free base porphyrins with zinc acetate in high yields. The hydrolysis of metal complexes was achieved by reacting metal complexes with excess aqueous KOH in a mixture solution of tetrahydrofuran (THF) and methanol. More synthetic details and characterization data of all porphyrins are included in the Supporting Information (SI). The *para*-carboxyphenyl-substituted porphyrins, Zn3TPA1A, *trans*-Zn2TPA2A, *cis*-Zn2TPA2A, and Zn1TPA3A, were also synthesized by the same methods; however, the synthetic details and characterization data for Zn3TPA1A, *cis*-Zn2TPA2A, and Zn1TPA3A were reported in our previous publications.[39,40] Details of the synthesis and characterization of *trans*-Zn2TPA2A are included in the SI.

Optical Spectroscopy. The UV−visible peak positions and molar absorption coefficients (ε) of the studied porphyrins measured in THF solution are listed in Table 1. All of the studied porphyrins exhibit typical metalloporphyrin features

DOI: 10.1021/am507503d
ACS Appl. Mater. Interfaces 2015, 7, 1879−1891

Chart 1. Molecular Structures of Meta- and Para-Series Porphyrins Used in This Study

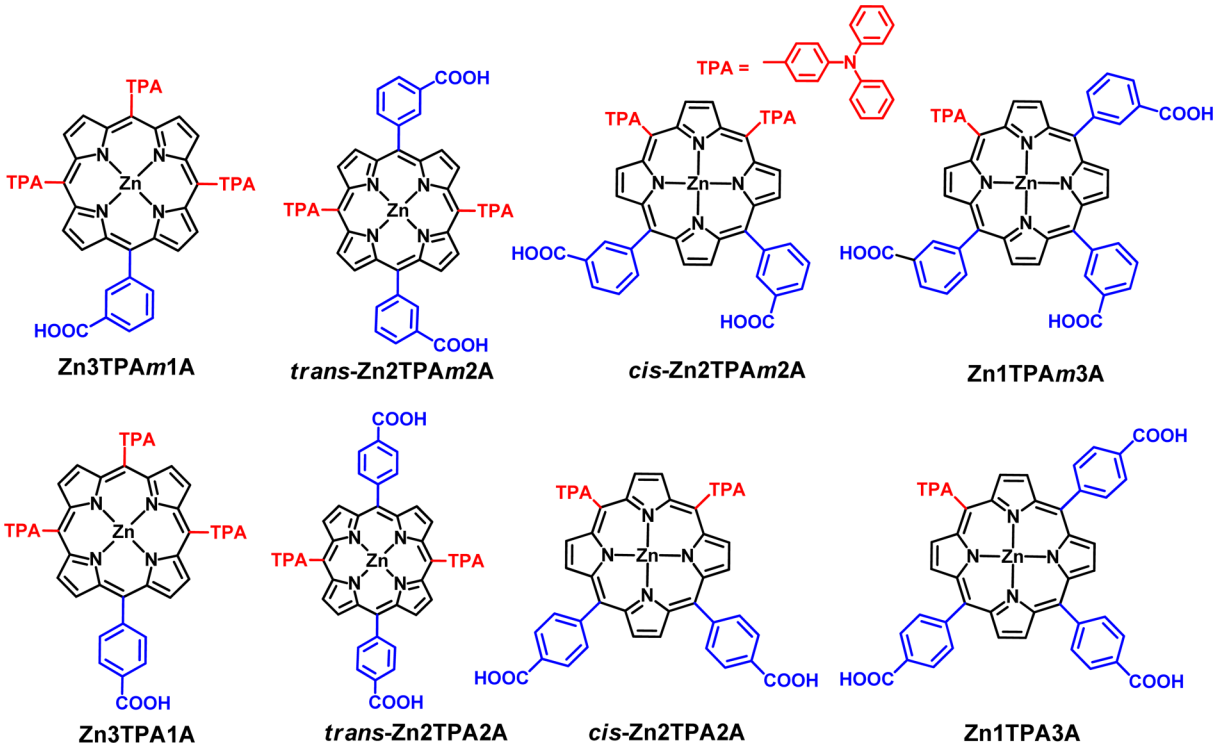

showing the presence of a single strong Soret band and two moderate Q bands (Figure S1, SI). The increasing number of TPA units gives broadening, and the red shift in the Soret band is attributed to the extended π-conjugation and inductive effect of TPA units. For example, in the meta series, the porphyrin sensitizer Zn3TPA*m*1A (434 nm) with three TPA units demonstrated a significant red shift compared to Zn1TPA*m*3A (427 nm). *trans*-Zn2TPA*m*2A (430 nm) and *cis*-Zn2TPA*m*2A (430 nm), both containing two TPA units, were red-shifted compared to the single-TPA-unit-containing Zn1TPA*m*3A (427 nm) but blue-shifted compared to the three-TPA-unit-containing Zn3TPA*m*1A (434 nm). A similar trend was observed for para-series porphyrins. The emission spectra of both series were measured in THF, and the emission maxima of the studied porphyrins are listed in Table 1. Similarly to the UV−visible spectra, the emission maxima show a red shift with increasing number of TPA units.

To understand the aggregation behavior of porphyrins on TiO_2, the thin-film spectra of the porphyrins were studied. The adsorbed porphyrin peaks show distinct behavior compared with that of their monomers in solvent. All of the porphyrins show broadening in the Soret and Q bands upon adsorption on TiO_2 (Figure S2, SI). In the meta series, the porphyrins *cis*-Zn2TPA*m*2A and Zn1TPA*m*3A show broadening with red shifts of 10 and 9 nm, respectively, whereas Zn3TPA*m*1A and *trans*-Zn2TPA*m*2A show broadening in the Soret band at the same wavelength. Figure 2a shows UV−visible spectra of *cis*-Zn2TPA*m*2A in THF compared with *cis*-Zn2TPA*m*2A adsorbed on TiO_2. The 10-nm red shift on TiO_2 indicates J-type aggregation.[30,41] In the para series, the porphyrins *trans*-Zn2TPA2A, *cis*-Zn2TPA2A, and Zn1TPA3A show 4-, 8-, and 5-nm red shifts, respectively, with broad shoulders in the blue-shift region, whereas the porphyrin Zn3TPA1A shows broadening at the Soret band only. Figure 2b shows UV−visible spectra of *cis*-Zn2TPA2A as a monomer in THF compared with *cis*-Zn2TPA2A adsorbed on TiO_2. The para-series porphyrins show more broadening than the meta-series porphyrins, implementing the optimal light harvesting that leads to higher power conversion efficiency.

Electrochemical Properties and Energy Levels. Cyclic voltammograms of the studied zinc porphyrins were measured in THF using 0.1 M $[TBA]PF_6$ the an electrolyte showed well-resolved and reversible oxidation potentials for all except *trans*-Zn2TPA2A (Figure S3, SI). The oxidation potentials of *trans*-Zn2TPA2A were determined using square-wave voltammetry. All of the studied porphyrins gave two successive oxidation steps, the first corresponding to one-electron oxidation of the TPA group and the second corresponding to one-electron oxidation of the porphyrin core.[42] The excited-state oxidation potentials (E_{ox}*) were calculated from the equation $E_{ox}^* = E_{ox} - E_{0-0}$, where E_{ox} is the first oxidation potential of the porphyrin dye and E_{0-0} is the zero−zero excitation energy obtained from the intersection of the absorption and emission bands. The HOMO energy level corresponding to the first oxidation potential and the LUMO energy level corresponding to E_{ox}* were used to plot energy level diagrams, which are displayed in Figure 3. It is noteworthy that, in the meta- and para-series porphyrin dyes, the HOMO−LUMO energy gaps remain almost invariable within a small range of 2.02−2.05 V, despite the fact that the numbers of TPA or carboxyphenyl units vary substantially. The energy level diagram demonstrates that the HOMO levels of all of the studied porphyrin dyes are more positive than that of the I^-/I_3^- redox couple electrolyte, which assures effective reductive regenerations of the oxidized porphyrin dyes in DSSC devices.

The LUMO energy levels (E_{ox}*) of the studied porphyrins are more negative than the CB of TiO_2, thus providing the necessary driving force for electron injection from the excited state of the dye into the CB of TiO_2. The driving force for

DOI: 10.1021/am507503d
ACS Appl. Mater. Interfaces 2015, 7, 1879−1891

Scheme 1. Synthesis of Zn3TPA*m*1A, *trans*-Zn2TPA*m*2A, *cis*-Zn2TPA*m*2A, and Zn1TPA*m*3A

(i) Mixed condensation

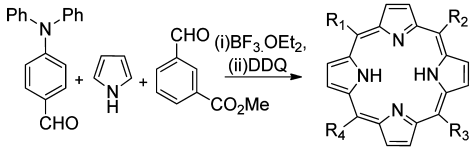

Pdt.	R_1	R_2	R_3	R_4
1.	TPA	TPA	TPA	CO_2Me
2.	TPA	CO_2Me	TPA	CO_2Me
3.	TPA	TPA	CO_2Me	CO_2Me
4.	TPA	CO_2Me	CO_2Me	CO_2Me

(ii) Zinc metalation

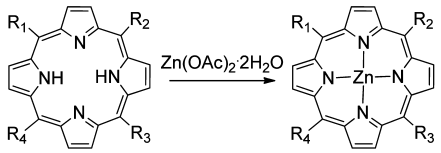

Pdt.	R_1	R_2	R_3	R_4
5.	TPA	TPA	TPA	CO_2Me
6.	TPA	CO_2Me	TPA	CO_2Me
7.	TPA	TPA	CO_2Me	CO_2Me
8.	TPA	CO_2Me	CO_2Me	CO_2Me

(iii)Hydrolysis

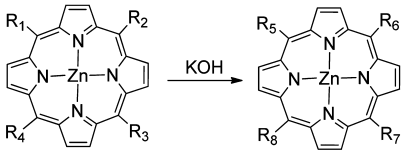

Dye	R_5	R_6	R_7	R_8
Zn3TPA*m*1A	TPA	TPA	TPA	CO_2H
trans-Zn2TPA*m*2A	TPA	CO_2H	TPA	CO_2H
cis-Zn2TPA*m*2A	TPA	TPA	CO_2H	CO_2H
Zn1TPA*m*3A	TPA	CO_2H	CO_2H	CO_2H

electron injection and dye regeneration of the studied dyes is sufficient to fulfill the requirements for effective DSSCs.

Density Functional Theory Calculations. To gain insights into the electron distribution of the frontier molecular orbitals of the studied porphyrins, density functional theory (DFT) calculations were performed with the Gaussian 09 package using the B3LYP functional and the 6-31G basis set.[43] The molecular orbitals were visualized using Chemoffice software (Chem 3D Ultra 2013). Results from the quantum chemical calculations are displayed in Figure 4. The phenyl rings at the meso positions of the porphyrins are twisted from the porphyrin plane by an average angle of 68°. All of the studied porphyrins show planar porphyrin macrocycle rings, which ensure effective electron coupling between the donor and acceptor units in the sensitizers. As seen in Figure 4, most of the electron density is accumulated over the electron-donating TPA groups in the HOMO − 1 and equally distributed over the TPA groups and the porphyrin rings in the HOMOs for both the meta and para series. Marked differences in the electron distributions for the meta- and para-series porphyrins are observed in the LUMOs. In the meta series, the electron density is localized almost exclusively over the porphyrin rings with only a slight portion extended over the *meta*-carboxyphenyl anchoring groups, whereas in the *para*-carboxyphenyl-substituted porphyrins, the majority of the electron density is distributed over the porphyrin rings with a significant portion extended over the carboxyphenyl groups, indicating that the charge separation in the para-series dyes is much better than that in the meta-series dyes. This improved charge separation in the para-series porphyrins might benefit intramolecular charge transfer (ICT) and consequently facilitate higher electron injection from the oxidized dye to the conduction band of the TiO_2. The overall superior performance of para- compared to meta-series dyes can also be explained on the basis of the observed dipole moments (μ) estimated by DFT calculations. For the para-series porphyrins, the values are in the order Zn1TPA3A (5.79 D) > *cis*-Zn2TPA2A (4.88 D) > Zn3TPA1A (3.59 D) > *trans*-Zn2TPA2A (2.59 D), and for the meta-series porphyrins, they are in the order Zn1TPA*m*3A (5.25 D) ≈ *cis*-Zn2TPA*m*2A

DOI: 10.1021/am507503d
ACS Appl. Mater. Interfaces 2015, 7, 1879−1891

Table 1. Optical and Electrochemical Properties of Porphyrins in THF

dye	λ_{abs} [a] (nm) (ε [10^3 M^{-1} cm^{-1}])	λ_{em} [b] (nm)	E_{ox} [c] (V)	E_{0-0} [d] (eV)	E_{ox}* [e] (V)
Zn3TPA*m*1A	434 (246)	622	0.90	2.03	−1.13
	561 (17)		1.08		
	604 (14)				
trans-Zn2TPA*m*2A	430 (309)	617	0.96	2.04	−1.08
	559 (23)	662	1.14		
	602 (15)				
cis-Zn2TPA*m*2A	430 (287)	614	0.95	2.03	−1.08
	560 (20)	662	1.13		
	602 (12)				
Zn1TPA*m*3A	427 (255)	610	1.05	2.05	−1.00
	559 (16)	658	1.26		
	599 (8)				
Zn3TPA1A	435 (137)	621	0.99	2.02	−1.03
	561 (8)		1.17		
	605 (7)				
trans-Zn2TPA2A	430 (280)	616	0.95	2.03	−1.08
	560 (21)	662	1.28		
	601 (14)				
cis-Zn2TPA2A[f]	430 (304)	616	1.05	2.04	−0.99
	560 (22)		1.22		
	602 (14)				
Zn1TPA3A[g]	427 (318)	611	1.07	2.04	- 0.97
	558 (21)	661	1.21		
	599 (12)				

[a]Absorption maximum of porphyrin in THF. [b]Emission maximum measured in THF by excitation at the Soret band. [c]First oxidation potentials determined using cyclic voltammetry in THF. [d]E_{0-0} values estimated from the intersection of the absorption and emission spectra. [e]E_{ox}*approximated from E_{ox} and E_{0-0}. [f]From ref 39. [g]From ref 40.

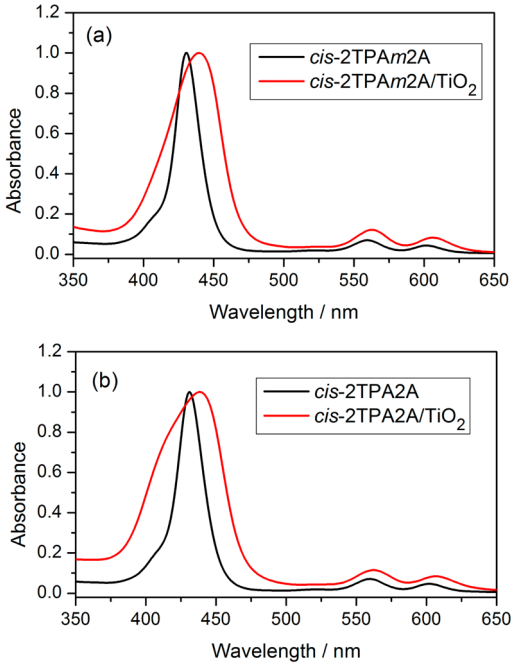

Figure 2. Comparative UV−visible spectra: (a) *cis*-Zn2TPA*m*2A versus *cis*-Zn2TPA*m*2A/TiO_2 and (b) *cis*-Zn2TPA2A versus *cis*-Zn2TPA2A/TiO_2.

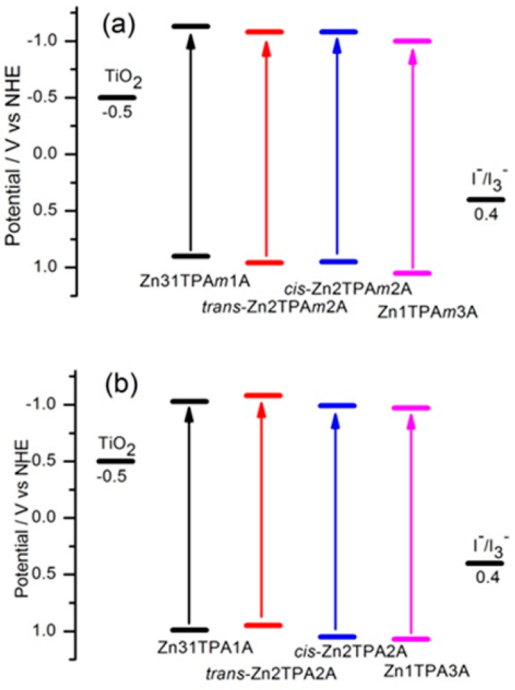

Figure 3. Energy level diagrams of (a) meta- and (b) para-series porphyrins.

(5.30 D) > Zn3TPA*m*1A (2.08 D) > *trans*-Zn2TPA*m*2A (1.22 D).

Attenuated Total Reflectance-Fourier Transform Infrared Spectroscopy. We used ATR-FTIR spectroscopy to evaluate the number of carboxyl units attached to TiO_2.[26,44−47] The ATR-FTIR spectra of neat porphyrin dyes were compared with those of the porphyrins adsorbed on TiO_2. The comparative spectra of the meta-series porphyrins contrasted with the same porphyrins adsorbed on TiO_2 are displayed in Figure 5. The ATR-FTIR spectra of Zn3TPA*m*1A, *trans*-

DOI: 10.1021/am507503d
ACS Appl. Mater. Interfaces 2015, 7, 1879−1891

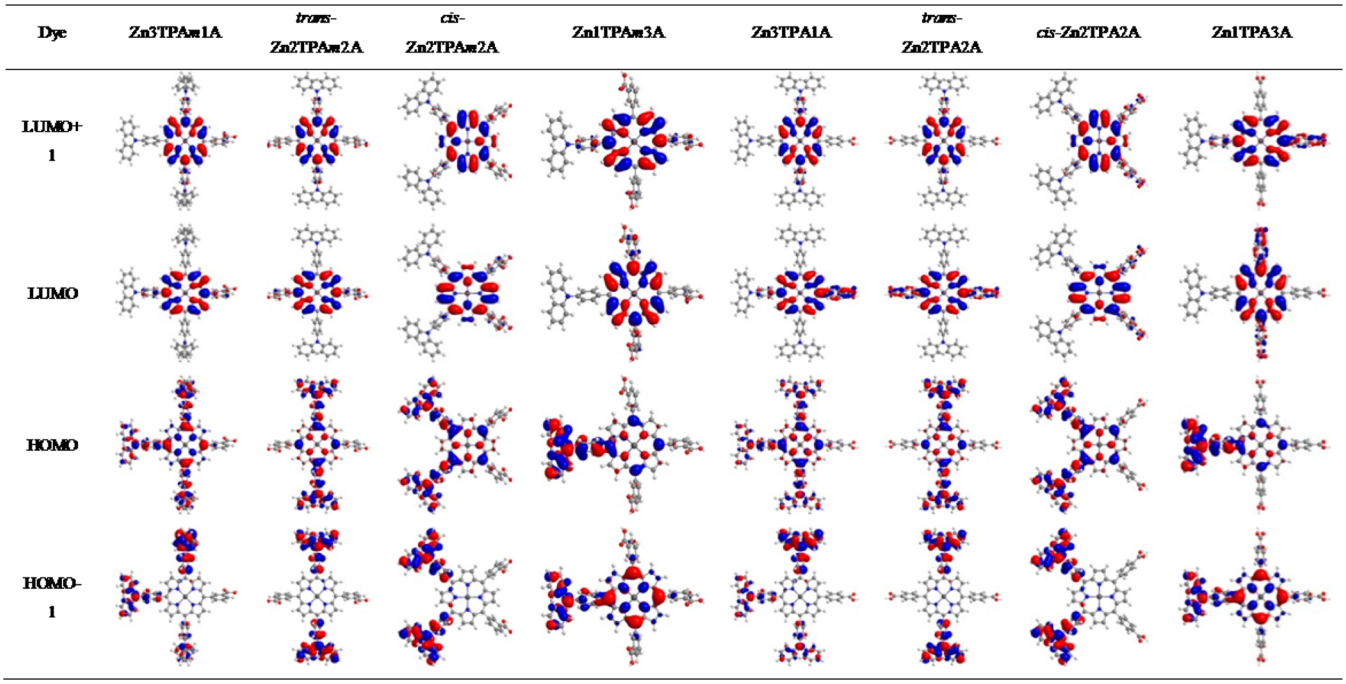

Figure 4. Molecular orbital diagrams of the studied porphyrins obtained from DFT calculations.

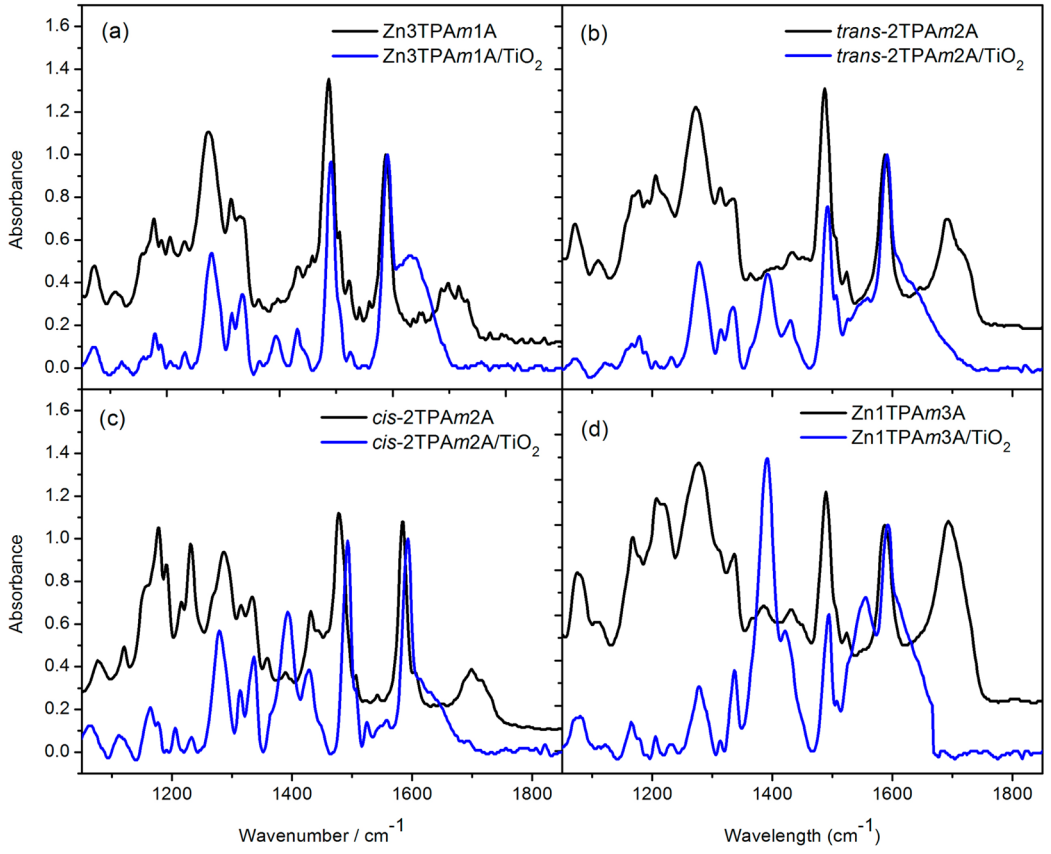

Figure 5. ATR-FTIR spectra of (a) Zn3TPA*m*1A and Zn3TPA*m*1A/TiO_2, (b) *trans*-Zn2TPA*m*2A and *trans*-Zn2TPA*m*2A/TiO_2, (c) *cis*-Zn2TPA*m*2A and *cis*-Zn2TPA*m*2A/TiO_2, and (d) Zn1TPA*m*3A and Zn1TPA*m*3A/TiO_2.

Zn2TPA*m*2A, *cis*-Zn2TPA*m*2A, and Zn1TPA*m*3A neat powders show very strong ν(C═O) stretching peaks at 1697, 1691, 1698, and 1693 cm^{-1}, respectively. In the comparative spectra of Zn3TPAm1A/TiO_2, *trans*-Zn2TPA*m*2A/TiO_2, *cis*-Zn2TPA-*m*2A/TiO_2, and Zn1TPA*m*3A/TiO_2, the ν(C═O) peaks disappear completely, and the $\nu_{sym}(COO^-)$ and $\nu_{asym}(COO^-)$ stretching peaks increase significantly, indicating the attachment of all carboxyl units onto the TiO_2. Figure 6 shows

DOI: 10.1021/am507503d
ACS Appl. Mater. Interfaces 2015, 7, 1879−1891

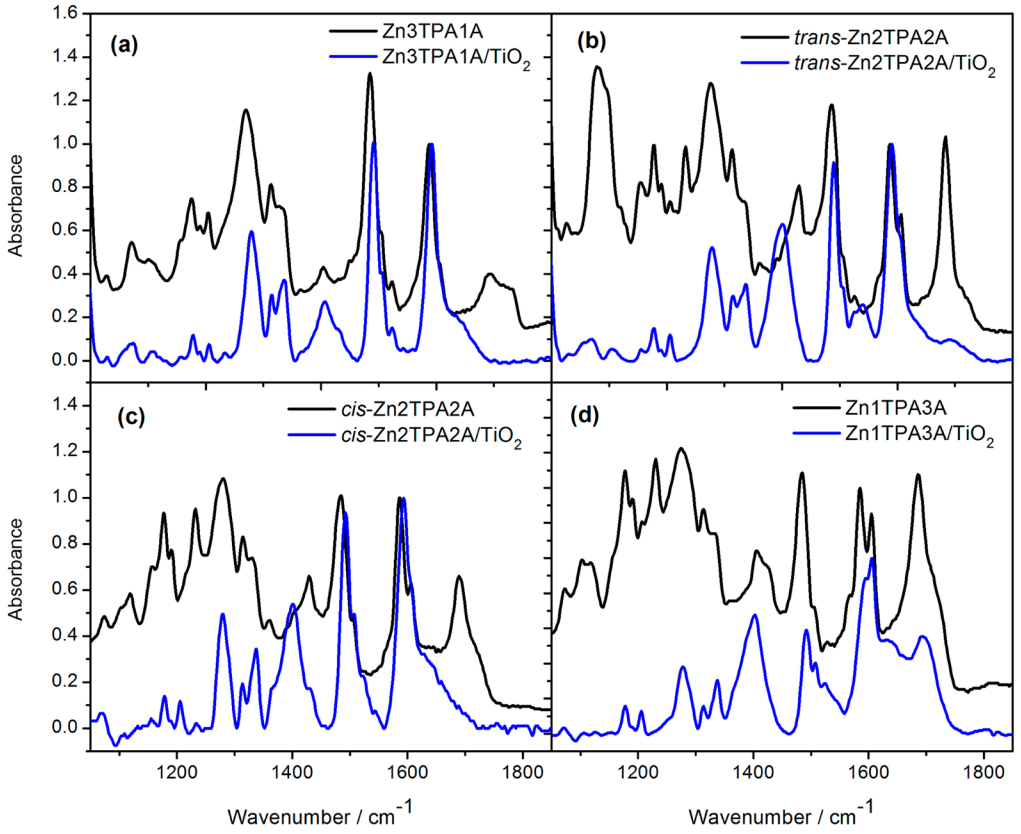

Figure 6. ATR-FTIR spectra of (a) Zn3TPA1A and Zn3TPA1A/TiO_2, (b) *trans*-Zn2TPA2A and *trans*-Zn2TPA2A/TiO_2, (c) *cis*-Zn2TPA2A and *cis*-Zn2TPA2A/TiO_2, and (d) Zn1TPA3A and Zn1TPA3A/TiO_2.

comparison spectra of neat para-series porphyrins with the same porphyrins adsorbed on TiO_2. The ATR-FTIR spectra of Zn3TPA1A, *trans*-Zn2TPA2A, *cis*-Zn2TPA2A, and Zn1TPA3A neat powders show very strong ν(C═O) stretching peaks at 1694, 1693, 1692, and 1686 cm^{-1}, respectively. In the comparative spectra of Zn3TPA1A/TiO_2 and *cis*-Zn2TPA2A/TiO_2, the ν(C═O) stretching peaks disappear completely, and the $\nu_{sym}(COO^-)$ and $\nu_{asym}(COO^-)$ stretching peaks increase noticeably, indicating that the available single carboxyl unit in Zn3TPA1A and two carboxyl units in *cis*-Zn2TPA2A are involved in attachment to TiO_2. On the contrary, the ATR-FTIR spectra of *trans*-Zn2TPA2A/TiO_2 and Zn1TPA3A//TiO_2 show marked increases in the $\nu_{sym}(COO^-)$ and $\nu_{asym}(COO^-)$ peaks, but the ν(C═O) stretching peaks at 1693 and 1686 cm^{-1} are still present with significant absorbance, suggesting the presence of a free unchelated *para*-carboxyphenyl unit. Based on these observations, the potential modes of attachment of *meta*-carboxyphenyl- and *para*-carboxyphenyl-series porphyrins on TiO_2 are shown in Figure 7. The meta derivatives Zn3TPA*m*1A and *cis*-Zn2TPA*m*2A, which can attach to the TiO_2 surface by one and two carboxyl anchors, respectively, might orient with large tilt angles rather than perpendicularly to the semiconductor surface, whereas *trans*-Zn2TPA*m*2A and Zn1TPA*m*3A, which attach to the TiO_2 surface by two and three carboxyl anchors, respectively, could lie flat on the TiO_2 surface because of structural geometries with loosely packed layers.[30] The tilted and flat orientations of meta derivatives bring the central zinc metal into close proximity with the TiO_2 surface, giving the electrons in the TiO_2 conduction band a chance to recombine faster with the oxidized dye.[48,49] It has been documented in the literature that organic and ruthenium dyes with a "push−pull" design and a small angle between the molecular plane and the TiO_2 surface would exhibit faster charge recombination, which would eventually reduce the overall conversion efficiency.[50,51] The superior performance of *cis*-Zn2TPA2A compared to *trans*-Zn2TPA2A can also be explained with the help of the ATR-FTIR measurements data. In the case of *cis*-Zn2TPA2A, both carboxyl groups participate in the binding with TiO_2, whereas in the case of *trans*-Zn2TPA2A, only one carboxyl group takes part in the binding with TiO_2.

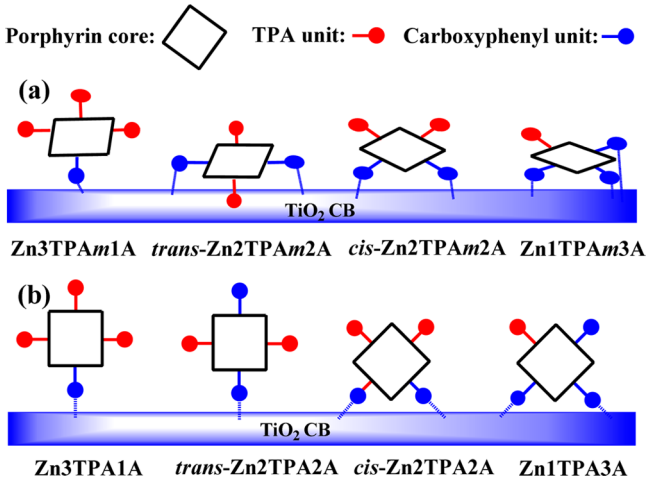

Figure 7. Possible modes of attachments of (a) meta- and (b) para-series porphyrins on TiO_2.

DOI: 10.1021/am507503d
ACS Appl. Mater. Interfaces 2015, 7, 1879−1891

Photovoltaic Measurements. Photovoltaic measurements of both series were performed under identical conditions and are summarized in Table 2. It was observed that the para-series

Table 2. Photovoltaic Properties of Meta- and Para-Series Porphyrins[a]

dye	J_{SC} (mA cm^{-2})	V_{OC} (V)	ff (%)	η (%)	dye loading (nmol cm^{-2})
Zn3TPA*m*1A	5.07	0.55	66	1.83	54
trans-Zn2TPA*m*2A	4.72	0.55	69	1.81	28
cis-Zn2TPA*m*2A	8.35	0.60	67	3.37	32
Zn1TPA*m*3A	9.00	0.60	69	3.72	38
Zn3TPA1A	7.86	0.56	65	2.88	81
trans-Zn2TPA2A	7.43	0.57	67	2.84	36
cis-Zn2TPA2A	10.48	0.59	65	4.02	81
Zn1TPA3A[b]	11.75	0.66	69	5.36	62
N719	16.57	0.74	67	8.23	-

[a]Identical conditions were applied for the photovoltaic measurements of both series, TiO_2 films were immersed in THF solution containing 2×10^{-4} M porphyrin and 2×10^{-4} M chenodeoxycholic acid (CDCA) at 50 °C for 30 min. [b]Efficiency data were taken from ref 40.

porphyrins are more efficient than the meta-series porphyrin analogues. The efficiency trend observed for meta-series porphyrins is Zn3TPA*m*1A ≈ *trans*-Zn2TPA*m*2A < *cis*-Zn2TPA*m*2A < Zn1TPA*m*3A. A similar trend of Zn3TPA1A ≈ *trans*-Zn2TPA2A < *cis*-Zn2TPA2A < Zn1TPA3A was observed for the para series as well. In the meta series, the highest efficiency of 3.72% was observed for Zn1TPA*m*3A followed by 3.37% for *cis*-Zn2TPA*m*2A, whereas *trans*-Zn2TPA*m*2A and Zn3TPA*m*1A gave similar efficiencies of 1.81% and 1.83%, respectively. In the para series, the highest efficiency of 5.36% was observed for Zn3TPA1A followed by *cis*-Zn2TPA2A at 4.02%, whereas the porphyrins *trans*-Zn2TPA2A and Zn3TPA1A gave similar efficiencies of 2.84% and 2.88%, respectively. The interrelation of efficiencies between the meta- and para-series porphyrin dyes can be described by the equation

$$\begin{array}{ccccccc} \text{Zn3TPA}m\text{1A} & \approx & \textit{trans}\text{-Zn2TPA}m\text{2A} & < & \textit{cis}\text{-Zn2TPA}m\text{2A} & < & \text{Zn1TPA}m\text{3A} \\ \wedge & & \wedge & & \wedge & & \wedge \\ \text{Zn3TPA1A} & \approx & \textit{trans}\text{-Zn2TPA2A} & < & \textit{cis}\text{-Zn2TPA2A} & < & \text{Zn1TPA3A} \end{array}$$

In general, the meta-series analogous porphyrins are less efficient than the para-series porphyrins despite the fact that they contain the same number of TPA and carboxyphenyl units; the only considered structural difference is the position of the *meta*- or *para*-carboxyl units. The meta-positioned carboxyphenyl units along with the bulky TPA units bring the porphyrin dye closer to the TiO_2 CB, through which a higher degree of charge recombination takes place, whereas the para-positioned carboxyphenyl units of the para-series porphyrins will likely achieve near-orthogonal orientations between the porphyrin planes and the TiO_2 surface, which allows for effective ICT and a higher efficiency. From the observed efficiency trends, it can be predicted that the para-series porphyrins with, presumably, orthogonal orientations have dominant charge injection and charge-transfer effects over charge recombination whereas the meta-series porphyrins with relative flat orientations have dominant charge recombination effects over charge injection and charge transfer.

The photocurrent−voltage (I−V) and IPCE curves of both series are shown in Figures 8 and 9, respectively. The relative order of IPCE values for the meta-series porphyrins is *trans*-

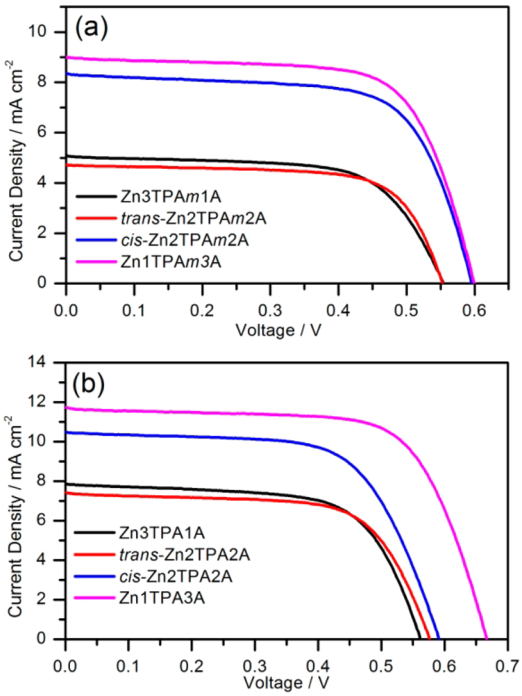

Figure 8. I−V curves of (a) meta- and (b) para-series porphyrins.

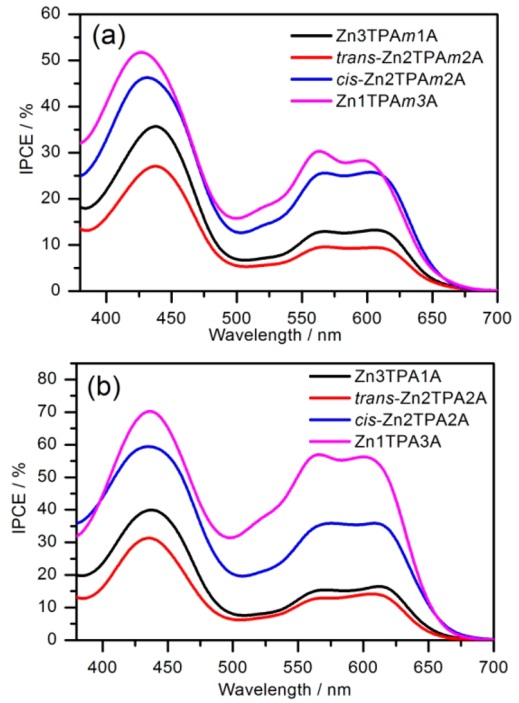

Figure 9. IPCE curves of (a) meta- and (b) para-series porphyrins.

Zn2TPA*m*2A < Zn3TPA*m*1A < *cis*-Zn2TPA*m*2A < Zn1TPA-*m*3A, and that for the para-series porphyrins is *trans*-Zn2TPA2A < Zn3TPA1A < *cis*-Zn2TPA2A < Zn1TPA3A. The IPCE trends observed here are exactly identical to the observed efficiency trends of both series. The IPCEs of the para-series porphyrins are comparatively higher than those of the meta-series porphyrins, which give higher electron injection yields, leading to higher efficiencies for the para-series porphyrins. In both series, the highest IPCE of 74% was achieved by Zn1TPA3A having the highest efficiency of 5.36%,

DOI: 10.1021/am507503d
ACS Appl. Mater. Interfaces 2015, 7, 1879−1891

followed by *cis*-Zn2TP2A with an IPCE of 60% and an efficiency of 4.02%, whereas the lowest IPCE of 33% was obtained by *trans*-Zn2TPA*m*2A having the lowest efficiency of 1.81%.

Electrochemical Impedance Spectroscopy. Electrochemical impedance spectroscopy (EIS) has been used as an important tool for understanding electron- and ion-transport processes in porphyrin-sensitized solar cells.[24,32,52−54] To gain more insight into the electron-transport process in the studied dyes, the EIS spectra of the studied porphyrin dyes were measured under one-sun illumination with an open-circuit voltage. The Nyquist plots of the studied porphyrins, shown in Figure 10, give one semicircle for each porphyrin.

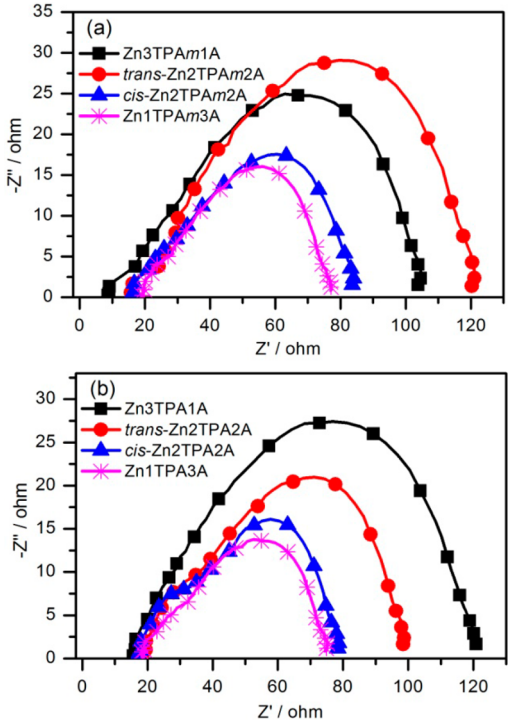

Figure 10. Nyquist plots of (a) meta- and (b) para-series porphyrins under one-sun illumination.

The observed semicircles correspond to the charge-transfer processes at the TiO_2−dye−electrolyte interface, that is, the electron-transport resistance.[55] A smaller radius of the semicircle in the Nyquist plot of one-sun illumination corresponds to a lower electron-transport resistance. The radii of the semicircles shown in Figure 10 and the observed efficiencies are inversely proportional to each other, indicating that the electron-transport resistance for the para-series porphyrins is lower than that for the meta-series porphyrins. The radii of the semicircles for the meta-series dyes are larger than those for the para-series dyes. In the meta-series derivatives, the radii of the porphyrins was observed to be in the order *trans*-Zn2TPA*m*2A > Zn3TPA*m*1A > *cis*-Zn2TPA*m*2A > Zn1TPA*m*3A, which is opposite to the order for efficiency. Porphyrin Zn1TPA*m*3A with the highest efficiency gives the smallest semicircle, and porphyrin Zn3TPA*m*1A with the lowest efficiency gives the largest semicircle, whereas in the para series, porphyrin Zn1TPA3A with the highest efficiency gives the smallest semicircle, and porphyrin Zn3TPA1A with a lower efficiency of 2.80% gives the largest semicircle. Overall, the obtained Nyquist plot data are in good agreement with the observed efficiency trends in both series.

Stability Study. The photostabilities of the meta- and para-series dyes were compared in terms of the UV−visible absorption spectra of the porphyrins on TiO_2. TiO_2 photoanode films of two dyes from the meta series, Zn3TPA*m*1A and Zn1TPA*m*3A, and two dyes from the para series, Zn3TPA1A and Zn1TPA3A, were irradiated under standard one-sun illumination for specific intervals of time. The UV−visible spectra of the studied dyes after irradiation for 0, 5, and 30 min were measured and are shown in Figure 11.

Upon irradiation, the meta-series dyes showed dramatic changes compared to the para-series dyes. Porphyrin Zn3TPA*m*1A exhibited a sharp decrease in absorption after irradiation for 30 min. Dyes with three carboxyphenyl groups, Zn1TPA*m*3A and Zn1TPA3A, showed higher stability than those with single carboxyphenyl groups, Zn3TPA*m*1A and Zn1TPA3A. Among the studied dyes, Zn3TPA*m*1A with a single *meta*-carboxyphenyl unit was observed to be the most unstable dye, whereas Zn1TPA3A with three *para*-carboxyphenyl units was found to be the most stable dye.

3. CONCLUSIONS

In conclusion, we have confirmed that the number and position of *meta*-carboxyphenyl and *para*-carboxyphenyl groups on the meso positons of porphyrin-based sensitizing dyes dramatically influence the performance of DSSCs in which these dyes are used. The performance of *para*-carboxyphenyl porphyrins is superior in all respects to that of *meta*-carboxyphenyl porphyrins. The compiled data from ATR-FTIR and EIS measurements reveal that, for meta-series porphyrins with large tilt angles or completely flat on TiO_2, charge recombination is dominant over charge injection, which leads to poor performance in comparison with the para series of porphyrins. In both the para and meta push−pull series, the *cis*-2A and 3A porphyrins, which are capable of injecting electrons through dual anchoring groups, give higher efficiencies. The photovoltaic parameters such as V_{OC}, J_{SC}, and IPCE of para-series porphyrins are distinctly superior to those of meta-series pophyrins and follow the same order of efficiency. Additionally, the photostability of the para-series porphyrins is higher than that of the meta-series porphyrins. In general, all of the *para*-carboxyphenyl derivatives outperform their *meta*-carboxyphenyl counterparts to achieve higher efficiencies and better device performance in DSSCs. The study reported herein will be useful for the design and development of efficient and stable sensitizers in DSSCs.

4. EXPERIMENTAL SECTION

Synthesis. The zinc porphyrins used in this study were synthesized in three steps, namely, mixed condensation, zinc metalation, and hydrolysis, by literature-reported methods. Detailed synthetic procedures for the target compounds with their characterization data are described in the SI. All of the porphyrins were characterized by optical spectroscopy, ATR-FTIR spectroscopy, nuclear magnetic resonance (NMR) spectroscopy, and high-resolution mass spectrometry. All chemicals were purchased from Acros Organics or Sigma-Aldrich and used without further purification. ^{1}H NMR spectra were recorded on a Bruker 400 MHz spectrometer in $CDCl_3$ (δ = 7.26 ppm), deuterated dimethyl sulfoxide (DMSO-d_6; δ = 2.50 ppm), or deuterated methanol (CD_4; δ = 3.31 ppm)

DOI: 10.1021/am507503d
ACS Appl. Mater. Interfaces 2015, 7, 1879−1891

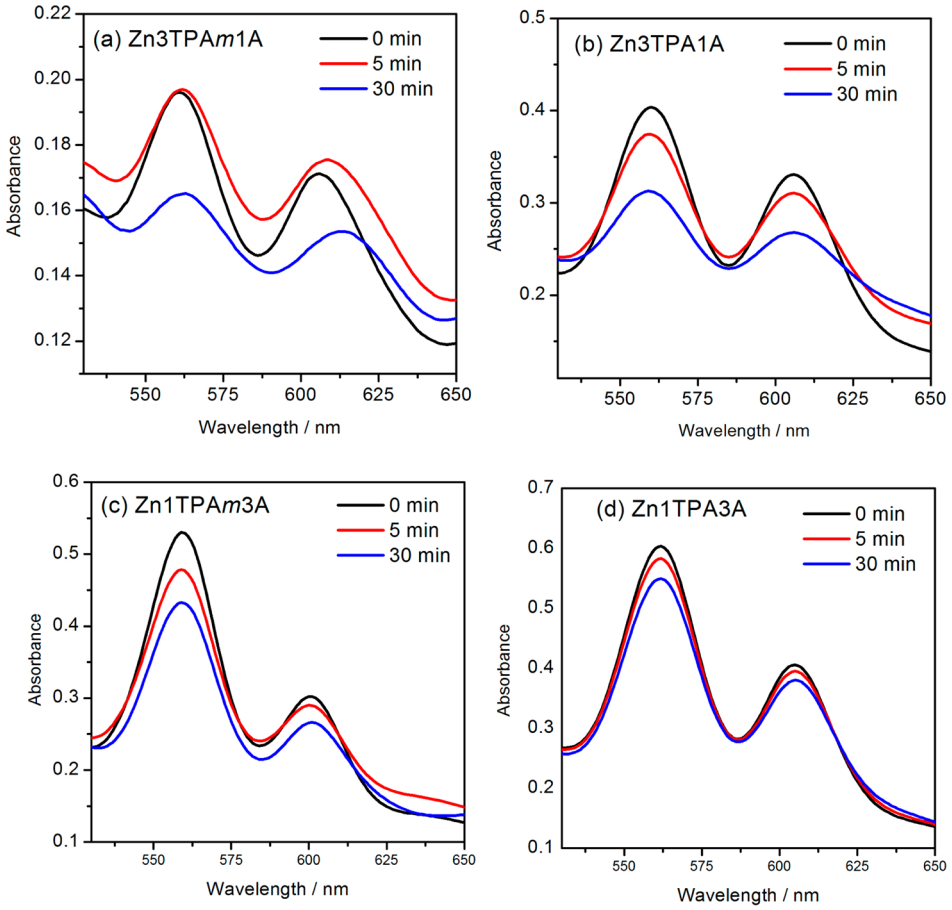

Figure 11. Absorption spectra of (a) Zn3TPA*m*1A, (b) Zn3TPA1A, (c) Zn1TPA*m*3A, and (d) Zn1TPA3A adsorbed onto TiO_2 films after irradiation for 0, 5, and 30 min.

solutions. Chemical shifts are reported in parts per million. Coupling constants *J* are reported in hertz. The signals are described as singlet, s; doublet, d; or doublet of doublets, dd. High-resolution mass spectrometry with fast atom bombardment (HRMS-FAB) or electrospray ionization (HRMS-ESI) was conducted on a JMS-700 double focusing mass spectrometer (JEOL, Tokyo, Japan). Flash chromatography was carried out using silica gel (40−63 μm, Merck). Analytical thin-layer chromatography (TLC) was performed on Merck silica gel plates. Melting points were recorded using an Electrothermal capillary melting point apparatus.

Optical Spectroscopy. UV−visible absorption spectra of the porphyrins in THF and adsorbed on TiO_2 electrodes were recorded using a JASCO V-670 UV−vis/NIR spectrophotometer. For the thin-film TiO_2 absorption spectra, 1 × 1 cm area TiO_2 films were prepared having a 3−4-μm thickness to obtain comparable shapes and positions of peaks. The films were immersed in 2×10^{-4} M porphyrin solutions in THF for 12 h; the films were then rinsed with THF and dried; and their absorbance was measured. Steady-state fluorescence spectra were acquired using a Varian Cary Eclipse fluorescence spectrophotometer.

Cyclic Voltammetry. Cyclic voltammetry measurements of all porphyrins were carried out on CHI 600D electrochemical analyzer (CH Instruments, Austin, TX) in degassed THF containing 0.1 M tetrabutylammonium hexafluorophosphate ($TBAPF_6$) as the supporting electrolyte. The cell assembly consisted of a glassy carbon as the working electrode, Ag wire as the reference electrode, and a platinum wire as the auxiliary electrode. The ferrocene/ferrocenium redox couple was used as an internal potential reference.

DFT Calculations. Density functional theory (DFT) calculations were performed with the Gaussian 09 package to study the electron distributions of the frontier molecular orbitals. All ground-state geometries of porphyrins were optimized in the gas phase using the hybrid B3LYP functional and the 6-31G basis set. The molecular orbitals were visualized using Chemoffice software (Chem 3D Ultra 2013).

ATR-FTIR Measurements. ATR-FTIR spectra of the zinc porphyrins were recorded on a VERTEX 70 spectrometer using a Golden Gate Diamond ATR accessory on solid powder porphyrin samples. For the preparation of samples with zinc porphyrins adsorbed on TiO_2, THF solution containing 5×10^{-4} M porphyrin was mixed with 5 mg of TiO_2 powder and held for 12 h, after which the excess solvent was dripped out by pipet. The TiO_2 powder was washed twice with THF and dried in a vacuum, and the obtained powder sample was used for measurement. ATR-FTIR spectra of zinc porphyrins adsorbed on TiO_2 were recorded at a resolution of 4 cm^{-1} and 320 scans.

Photovoltaic Measurements. The TiO_2 photoanode (product OPV-TiO_2-SP) and Pt counter electrode (product OPV-Pt-P) films were purchased from Yingkou Opvtech New Energy Co. Ltd. (Liaoning, China). The TiO_2 films, which were prepared by a screen-printing method, were composed of a transparent layer (thickness ≈ 12 μm) and a scattering layer (thickness ≈ 4 μm) and had a working area of 0.4 × 0.4 cm^2,

DOI: 10.1021/am507503d
ACS Appl. Mater. Interfaces 2015, 7, 1879−1891

and they were used directly upon receipt. The films were pretreated by the following activation procedures before use: heating at 100 °C for 22 min, at 110 °C for 60 min, at 450 °C for 68 min, at 500 °C 60 min, and at 250 °C for 60 min; cooling to 80 °C and holding at 80 °C before immersion. The TiO_2 films were immersed in THF solution containing 2×10^{-4} M porphyrin and 2×10^{-4} M chenodeoxycholic acid (CDCA) at 50 °C for 30 min. The dye-sensitized TiO_2 films were washed with THF, dried with hot air, and used as working electrodes. The Pt counter electrodes were used directly as received. To fabricate the DSSC devices, the two electrodes were tightly clipped together into a sandwich-type cell, spaced by a 40-μm film spacer. A thin layer of electrolyte containing 0.05 M I_2, 0.1 M lithium iodide (LiI), 0.6 M 1,2-dimethyl-3-propylimidazolium iodide (DMPII), and 0.6 M 4-*tert*-butylpyridine (TBP) in dry CH_3CN was introduced into the space between the two electrodes. The photoelectrochemical characterizations on the solar cells were carried out using an Oriel Class A solar simulator (Oriel 91195A, Newport Corp.). Photocurrent−voltage characteristics of the DSSCs were recorded with a potentiostat/galvanostat (CHI650B, CH Instruments, Inc.) at a light intensity of 100 mW cm^{-2} calibrated with an Oriel reference solar cell (Oriel 91150, Newport Corp.). The monochromatic quantum efficiency was recorded through a monochromator (Oriel 74100, Newport Corp.) under short-circuit conditions. The intensity of each wavelength was in the range of 1−3 mW cm^{-2}. The porphyrins on TiO_2 films were desorbed using 0.2 M aqueous KOH in THF, and the absorbance was measured to determine the dye loading density.

Stability Study. For the stability study, TiO_2 thin films having a 1×1 cm^2 area and a 3−4-μm thickness were used. The films were immersed in 2×10^{-4} M porphyrin in THF for 0.5 h and dried, and the absorbance was measured. The same films were irradiated under standard one-sun illumination for 5 and 30 min, and the absorbance was measured again.

■ ASSOCIATED CONTENT

Ⓢ Supporting Information

Synthesis, characterization data, and NMR and HRMS spectra of all the new porphyrins Zn3TPA*m*1A, *trans*-Zn2TPA*m*2A, *cis*-Zn2TPA*m*2A, Zn1TPA*m*3A, and *trans*-Zn2TPA2A. This material is available free of charge via the Internet at http://pubs.acs.org.

■ AUTHOR INFORMATION

Corresponding Author

*E-mail: chhung@gate.sinica.edu.tw. Tel.: +88627898570.

Notes

The authors declare no competing financial interest.

■ ACKNOWLEDGMENTS

The authors gratefully acknowledge the financial support from the National Science Council (Taiwan) and Academia Sinica. Mass spectroscopy analyses were performed by the Mass Spectrometry facility of the Institute of Chemistry, Academia Sinica, Taipei, Taiwan. The help from Dr. Jiann-T'suen Lin on the measurements and instrumentations is greatly appreciated.

■ REFERENCES

(1) O'Regan, B.; Grätzel, M. A Low-Cost, High-Efficiency Solar Cell based on Dye-Sensitized Colloidal TiO_2 Films. *Nature* **1991**, *353*, 737−740.
(2) Gratzel, M. Photoelectrochemical Cells. *Nature* **2001**, *414*, 338−344.
(3) Hagfeldt, A.; Boschloo, G.; Sun, L.; Kloo, L.; Pettersson, H. Dye-Sensitized Solar Cells. *Chem. Rev.* **2010**, *110*, 6595−663.
(4) Li, L.-L.; Diau, E. W.-G. Porphyrin-Sensitized Solar Cells. *Chem. Soc. Rev.* **2013**, *42*, 291−304.
(5) Campbell, W. M.; Burrell, A. K.; Officer, D. L.; Jolley, K. W. Porphyrins as Light Harvesters in the Dye-Sensitised TiO_2 Solar Cell. *Coord. Chem. Rev.* **2004**, *248*, 1363−1379.
(6) Kira, A.; Matsubara, Y.; Iijima, H.; Umeyama, T.; Matano, Y.; Ito, S.; Niemi, M.; Tkachenko, N. V.; Lemmetyinen, H.; Imahori, H. Effects of π-Elongation and the Fused Position of Quinoxaline-Fused Porphyrins as Sensitizers in Dye-Sensitized Solar Cells on Optical, Electrochemical, and Photovoltaic Properties. *J. Phys. Chem. C* **2010**, *114*, 11293−11304.
(7) Martinez-Diaz, M. V.; de la Torrea, G.; Torres, T. Lighting Porphyrins and Phthalocyanines for Molecular Photovoltaics. *Chem. Commun.* **2010**, *46*, 7090−7108.
(8) Han, L.; Islam, A.; Chen, H.; Malapaka, C.; Chiranjeevi, B.; Zhang, S.; Yang, X.; Yanagida, M. High-Efficiency Dye-Sensitized Solar Cell with a Novel Co-adsorbent. *Energy Environ. Sci.* **2012**, *5*, 6057−6060.
(9) Nazeeruddin, M. K.; De Angelis, F.; Fantacci, S.; Selloni, A.; Viscardi, G.; Liska, P.; Ito, S.; Takeru, B.; Grätzel, M. Combined Experimental and DFT-TDDFT Computational Study of Photoelectrochemical Cell Ruthenium Sensitizers. *J. Am. Chem. Soc.* **2005**, *127*, 16835−16847.
(10) Gao, F.; Wang, Y.; Shi, D.; Zhang, J.; Wang, M.; Jing, X.; Humphry-Baker, R.; Wang, P.; Zakeeruddin, S. M.; Grätzel, M. Enhance the Optical Absorptivity of Nanocrystalline TiO_2 Film with High Molar Extinction Coefficient Ruthenium Sensitizers for High Performance Dye-Sensitized Solar Cells. *J. Am. Chem. Soc.* **2008**, *130*, 10720−10728.
(11) Bai, Y.; Zhang, J.; Zhou, D.; Wang, Y.; Zhang, M.; Wang, P. Engineering Organic Sensitizers for Iodine-Free Dye-Sensitized Solar Cells: Red-Shifted Current Response Concomitant with Attenuated Charge Recombination. *J. Am. Chem. Soc.* **2011**, *133*, 11442−11445.
(12) Joly, D.; Pellejà, L.; Narbey, S.; Oswald, F.; Chiron, J.; Clifford, J. N.; Palomares, E.; Demadrille, R. A Robust Organic Dye for Dye Sensitized Solar Cells Based on Iodine/Iodide Electrolytes Combining High Efficiency and Outstanding Stability. *Sci. Rep.* **2014**, *4*, 4033.
(13) Wu, Y.; Marszalek, M.; Zakeeruddin, S. M.; Zhang, Q.; Tian, H.; Gratzel, M.; Zhu, W. High-Conversion-Efficiency Organic Dye-Sensitized Solar Cells: Molecular Engineering on D−A−π−A Featured Organic Indoline Dyes. *Energy Environ. Sci.* **2012**, *5*, 8261−8272.
(14) Bessho, T.; Zakeeruddin, S. M.; Yeh, C.-Y.; Diau, E. W.-G.; Grätzel, M. Highly Efficient Mesoscopic Dye-Sensitized Solar Cells Based on Donor−Acceptor-Substituted Porphyrins. *Angew. Chem., Int. Ed.* **2010**, *49*, 6646−6649.
(15) Wu, S.-L.; Lu, H.-P.; Yu, H.-T.; Chuang, S.-H.; Chiu, C.-L.; Lee, C.-W.; Diau, E. W.-G.; Yeh, C.-Y. Design and Characterization of Porphyrin Sensitizers with a Push-Pull Framework for Highly Efficient Dye-Sensitized Solar Cells. *Energy Environ. Sci.* **2010**, *3*, 949−955.
(16) Imahori, H.; Matsubara, Y.; Iijima, H.; Umeyama, T.; Matano, Y.; Ito, S.; Niemi, M.; Tkachenko, N. V.; Lemmetyinen, H. Effects of *meso*-Diarylamino Group of Porphyrins as Sensitizers in Dye-Sensitized Solar Cells on Optical, Electrochemical, and Photovoltaic Properties. *J. Phys. Chem. C* **2010**, *114*, 10656−10665.
(17) Eu, S.; Hayashi, S.; Umeyama, T.; Oguro, A.; Kawasaki, M.; Kadota, N.; Matano, Y.; Imahori, H. Effects of 5-Membered Heteroaromatic Spacers on Structures of Porphyrin Films and Photovoltaic Properties of Porphyrin-Sensitized TiO_2 Cells. *J. Phys. Chem. C* **2007**, *111*, 3528−3537.
(18) Wang, C.-L.; Chang, Y.-C.; Lan, C.-M.; Lo, C.-F.; Wei-Guang Diau, E.; Lin, C.-Y. Enhanced Light Harvesting with π-Conjugated

DOI: 10.1021/am507503d
ACS Appl. Mater. Interfaces 2015, 7, 1879−1891

Cyclic Aromatic Hydrocarbons for Porphyrin-Sensitized Solar Cells. *Energy Environ. Sci.* **2011**, *4*, 1788−1795.
(19) Lan, C.-M.; Wu, H.-P.; Pan, T.-Y.; Chang, C.-W.; Chao, W.-S.; Chen, C.-T.; Wang, C.-L.; Lin, C.-Y.; Diau, E. W.-G. Enhanced Photovoltaic Performance with Co-sensitization of Porphyrin and an Organic Dye in Dye-Sensitized Solar Cells. *Energy Environ. Sci.* **2012**, *5*, 6460−6464.
(20) Kurotobi, K.; Toude, Y.; Kawamoto, K.; Fujimori, Y.; Ito, S.; Chabera, P.; Sundström, V.; Imahori, H. Highly Asymmetrical Porphyrins with Enhanced Push−Pull Character for Dye-Sensitized Solar Cells. *Chem.—Eur. J.* **2013**, *19*, 17075−17081.
(21) Imahori, H.; Umeyama, T.; Ito, S. Large π-Aromatic Molecules as Potential Sensitizers for Highly Efficient Dye-Sensitized Solar Cells. *Acc. Chem. Res.* **2009**, *42*, 1809−1818.
(22) Higashino, T.; Imahori, H. Porphyrins as Excellent Dyes for Dye-Sensitized Solar Cells: Recent Developments and Insights. *Dalton Trans.* **2015**, *44*, 448−463.
(23) Liu, Y.; Xiang, N.; Feng, X.; Shen, P.; Zhou, W.; Weng, C.; Zhao, B.; Tan, S. Thiophene-Linked Porphyrin Derivatives for Dye-Sensitized Solar Cells. *Chem. Commun.* **2009**, 2499−2501.
(24) Panda, M. K.; Sharma, G. D.; Justin Thomas, K. R.; Coutsolelos, A. G. A New Family of A_2B_2 Type Porphyrin Derivatives: Synthesis, Physicochemical Characterization and Their Application in Dye-Sensitized Solar Cells. *J. Mater. Chem.* **2012**, *22*, 8092−8102.
(25) Campbell, W. M.; Jolley, K. W.; Wagner, P.; Wagner, K.; Walsh, P. J.; Gordon, K. C.; Schmidt-Mende, L.; Nazeeruddin, M. K.; Wang, Q.; Grätzel, M.; Officer, D. L. Highly Efficient Porphyrin Sensitizers for Dye-Sensitized Solar Cells. *J. Phys. Chem. C* **2007**, *111*, 11760−11762.
(26) Nazeeruddin, M. K.; Humphry-Baker, R.; Officer, D. L.; Campbell, W. M.; Burrell, A. K.; Grätzel, M. Application of Metalloporphyrins in Nanocrystalline Dye-Sensitized Solar Cells for Conversion of Sunlight into Electricity. *Langmuir* **2004**, *20*, 6514−6517.
(27) Yella, A.; Mai, C.-L.; Zakeeruddin, S. M.; Chang, S.-N.; Hsieh, C.-H.; Yeh, C.-Y.; Grätzel, M. Molecular Engineering of Push−Pull Porphyrin Dyes for Highly Efficient Dye-Sensitized Solar Cells: The Role of Benzene Spacers. *Angew. Chem., Int. Ed.* **2014**, *53*, 2973−2977.
(28) Mathew, S.; Yella, A.; Gao, P.; Humphry-Baker, R.; CurchodBasile, F. E.; Ashari-Astani, N.; Tavernelli, I.; Rothlisberger, U.; NazeeruddinMd, K.; Grätzel, M. Dye-Sensitized Solar Cells with 13% Efficiency Achieved through the Molecular Engineering of Porphyrin Sensitizers. *Nat. Chem.* **2014**, *6*, 242−247.
(29) Odobel, F.; Blart, E.; Lagree, M.; Villieras, M.; Boujtita, H.; El Murr, N.; Caramori, S.; Alberto Bignozzi, C. Porphyrin Dyes for TiO_2 Sensitization. *J. Mater. Chem.* **2003**, *13*, 502−510.
(30) Rochford, J.; Chu, D.; Hagfeldt, A.; Galoppini, E. Tetrachelate Porphyrin Chromophores for Metal Oxide Semiconductor Sensitization: Effect of the Spacer Length and Anchoring Group Position. *J. Am. Chem. Soc.* **2007**, *129*, 4655−4665.
(31) Lee, C.-W.; Lu, H.-P.; Lan, C.-M.; Huang, Y.-L.; Liang, Y.-R.; Yen, W.-N.; Liu, Y.-C.; Lin, Y.-S.; Diau, E. W.-G.; Yeh, C.-Y. Novel Zinc Porphyrin Sensitizers for Dye-Sensitized Solar Cells: Synthesis and Spectral, Electrochemical, and Photovoltaic Properties. *Chem.—Eur. J.* **2009**, *15*, 1403−1412.
(32) Hart, A. S.; Kc, C. B.; Gobeze, H. B.; Sequeira, L. R.; D'Souza, F. Porphyrin-Sensitized Solar Cells: Effect of Carboxyl Anchor Group Orientation on the Cell Performance. *ACS Appl. Mater. Interfaces* **2013**, *5*, 5314−5323.
(33) Zhang, L.; Cole, J. M.; Waddell, P. G.; Low, K. S.; Liu, X. Relating Electron Donor and Carboxylic Acid Anchoring Substitution Effects in Azo Dyes to Dye-Sensitized Solar Cell Performance. *ACS Sustainable Chem. Eng.* **2013**, *1*, 1440−1452.
(34) Si, L.; He, H. Porphyrin Dyes on TiO_2 Surfaces with Different Orientations: A Photophysical, Photovoltaic, and Theoretical Investigation. *J. Phys. Chem. A* **2014**, *118*, 3410−3418.
(35) Mane, S. B.; Luo, L.; Chang, G.-F.; Diau, E. W.-G.; Hung, C.-H. Effects of Core-Modification on Porphyrin Sensitizers to the Efficiencies of Dye-Sensitized Solar Cells. *J. Chin. Chem. Soc.* **2014**, *61*, 545−555.
(36) Mane, S. B.; Hung, C.-H. Synthesis of Carboxylate Functionalized A_3B and A_2B_2 Thiaporphyrins and Their Application in Dye-Sensitized Solar Cells. *New J. Chem.* **2014**, *38*, 3960−3972.
(37) Mane, S. B.; Hu, J.-Y.; Chang, Y.-C.; Luo, L.; Diau, E. W.-G.; Hung, C.-H. Novel Expanded Porphyrin Sensitized Solar Cells Using Boryl Oxasmaragdyrin as the Sensitizer. *Chem. Commun.* **2013**, *49*, 6882−6884.
(38) Ambre, R.; Chen, K.-B.; Yao, C.-F.; Luo, L.; Diau, E. W.-G.; Hung, C.-H. Effects of Porphyrinic *meso*-Substituents on the Photovoltaic Performance of Dye-Sensitized Solar Cells: Number and Position of *p*-Carboxyphenyl and Thienyl Groups on Zinc Porphyrins. *J. Phys. Chem. C* **2012**, *116*, 11907−11916.
(39) Ambre, R. B.; Chang, G.-F.; Zanwar, M. R.; Yao, C.-F.; Diau, E. W.-G.; Hung, C.-H. New Dual Donor−Acceptor (2D-π-2A) Porphyrin Sensitizers for Stable and Cost-Effective Dye-Sensitized Solar Cells. *Chem. Asian. J.* **2013**, *8*, 2144−2153.
(40) Ambre, R. B.; Chang, G.-F.; Hung, C.-H. Three *p*-Carboxyphenyl Groups Possessing Zinc Porphyrins: Efficient, Stable, and Cost-Effective Sensitizers for Dye-Sensitized Solar Cells. *Chem. Commun.* **2014**, *50*, 725−727.
(41) Roales, J.; Pedrosa, J. M.; Cano, M.; Guillen, M. G.; Lopes-Costa, T.; Castillero, P.; Barranco, A.; Gonzalez-Elipe, A. R. Anchoring Effect on (Tetra)Carboxyphenyl Porphyrin/TiO_2 Composite Films for VOC Optical Detection. *RSC Adv.* **2014**, *4*, 1974−1981.
(42) Hsieh, C.-P.; Lu, H.-P.; Chiu, C.-L.; Lee, C.-W.; Chuang, S.-H.; Mai, C.-L.; Yen, W.-N.; Hsu, S.-J.; Diau, E. W.-G.; Yeh, C.-Y. Synthesis and Characterization of Porphyrin Sensitizers with Various Electron-Donating Substituents for Highly Efficient Dye-Sensitized Solar Cells. *J. Mater. Chem.* **2010**, *20*, 1127−1134.
(43) Frisch, M. J.; Trucks, G. W.; Schlegel, H. B.; Scuseria, G. E.; Robb, M. A.; Cheeseman, J. R.; Scalmani, G.; Barone, V.; Mennucci, B.; Petersson, G. A.; Nakatsuji, H.; Caricato, M.; Li, X.; Hratchian, H. P.; Izmaylov, A. F.; Bloino, J.; Zheng, G.; Sonnenberg, J. L.; Hada, M.; Ehara, M.; Toyota, K.; Fukuda, R.; Hasegawa, J.; Ishida, M.; Nakajima, T.; Honda, Y.; Kitao, O.; Nakai, H.; Vreven, T.; Montgomery, J. A., Jr.; Peralta, J. E.; Ogliaro, F.; Bearpark, M.; Heyd, J. J.; Brothers, E.; Kudin, K. N.; Staroverov, V. N.; Keith, T.; Kobayashi, R.; Normand, J.; Raghavachari, K.; Rendell, A.; Burant, J. C.; Iyengar, S. S.; Tomasi, J.; Cossi, M.; Rega, N.; Millam, J. M.; Klene, M.; Knox, J. E.; Cross, J. B.; Bakken, V.; Adamo, C.; Jaramillo, J.; Gomperts, R.; Stratmann, R. E.; Yazyev, O.; Austin, A. J.; Cammi, R.; Pomelli, C.; Ochterski, J. W.; Martin, R. L.; Morokuma, K.; Zakrzewski, V. G.; Voth, G. A.; Salvador, P.; Dannenberg, J. J.; Dapprich, S.; Daniels, A. D.; Farkas, Ö.; Foresman, J. B.; Ortiz, J. V.; Cioslowski, J.; Fox, D. J. *Gaussian 09, Revision D.01*; Gaussian, Inc.: Wallingford, CT, 2009.
(44) Bouit, P.-A.; Marszalek, M.; Humphry-Baker, R.; Viruela, R.; Ortí, E.; Zakeeruddin, S. M.; Grätzel, M.; Delgado, J. L.; Martín, N. Donor-π-Acceptors Containing the 10-(1,3-Dithiol-2-ylidene)-anthracene Unit for Dye-Sensitized Solar Cells. *Chem.—Eur. J.* **2012**, *18*, 11621−11629.
(45) Abbotto, A.; Manfredi, N.; Marinzi, C.; De Angelis, F.; Mosconi, E.; Yum, J.-H.; Xianxi, Z.; Nazeeruddin, M. K.; Gratzel, M. Di-Branched Di-Anchoring Organic Dyes for Dye-Sensitized Solar Cells. *Energy Environ. Sci.* **2009**, *2*, 1094−1101.
(46) Lu, N.; Shing, J.-S.; Tu, W.-H.; Hsu, Y.-C.; Lin, J. T. Novel Fluorous Amphiphilic Heteroleptic Ru-Based Complexes for a Dye-Sensitized Solar Cell: The First Fluorous Bis-ponytailed Amphiphilic Ru Complexes. *Inorg. Chem.* **2011**, *50*, 4289−4294.
(47) Heredia, D.; Natera, J.; Gervaldo, M.; Otero, L.; Fungo, F.; Lin, C.-Y.; Wong, K.-T. Spirobifluorene-Bridged Donor/Acceptor Dye for Organic Dye-Sensitized Solar Cells. *Org. Lett.* **2009**, *12*, 12−15.
(48) Imahori, H.; Kang, S.; Hayashi, H.; Haruta, M.; Kurata, H.; Isoda, S.; Canton, S. E.; Infahsaeng, Y.; Kathiravan, A.; Pascher, T. r.; Chábera, P.; Yartsev, A. P.; Sundström, V. Photoinduced Charge Carrier Dynamics of Zn−Porphyrin−TiO_2 Electrodes: The Key Role of Charge Recombination for Solar Cell Performance. *J. Phys. Chem. A* **2010**, *115*, 3679−3690.

DOI: 10.1021/am507503d
ACS Appl. Mater. Interfaces 2015, 7, 1879−1891

(49) Ye, S.; Kathiravan, A.; Hayashi, H.; Tong, Y.; Infahsaeng, Y.; Chabera, P.; Pascher, T.; Yartsev, A. P.; Isoda, S.; Imahori, H.; Sundström, V. Role of Adsorption Structures of Zn-Porphyrin on TiO_2 in Dye-Sensitized Solar Cells Studied by Sum Frequency Generation Vibrational Spectroscopy and Ultrafast Spectroscopy. *J. Phys. Chem. C* **2013**, *117*, 6066−6080.
(50) Pastore, M.; De Angelis, F. Computational Modelling of TiO_2 Surfaces Sensitized by Organic Dyes with Different Anchoring Groups: Adsorption Modes, Electronic Structure and Implication for Electron Iinjection/Recombination. *Phys. Chem. Chem. Phys.* **2012**, *14*, 920−928.
(51) Clifford, J. N.; Palomares, E.; Nazeeruddin, M. K.; Grätzel, M.; Nelson, J.; Li, X.; Long, N. J.; Durrant, J. R. Molecular Control of Recombination Dynamics in Dye-Sensitized Nanocrystalline TiO_2 Films: Free Energy vs Distance Dependence. *J. Am. Chem. Soc.* **2004**, *126*, 5225−5233.
(52) Daphnomili, D.; Landrou, G.; Prakash Singh, S.; Thomas, A.; Yesudas, K.; K, B.; Sharma, G. D.; Coutsolelos, A. G. Photophysical, Electrochemical and Photovoltaic Properties of Dye Sensitized Solar Cells Using a Series of Pyridyl Functionalized Porphyrin Dyes. *RSC Adv.* **2012**, *2*, 12899−12908.
(53) Liu, B.; Zhu, W.; Wang, Y.; Wu, W.; Li, X.; Chen, B.; Long, Y.-T.; Xie, Y. Modulation of Energy Levels by Donor Groups: An Effective Approach for Optimizing the Efficiency of Zinc-Porphyrin Based Solar Cells. *J. Mater. Chem.* **2012**, *22*, 7434−7444.
(54) Mikroyannidis, J. A.; Charalambidis, G.; Coutsolelos, A. G.; Balraju, P.; Sharma, G. D. Novel Zinc Porphyrin with Phenylenevinylene *meso*-Substituents: Synthesis and Application in Dye-Sensitized Solar Cells. *J. Power Sources* **2011**, *196*, 6622−6628.
(55) Yang, C.-J.; Chang, Y. J.; Watanabe, M.; Hon, Y.-S.; Chow, T. J. Phenothiazine Derivatives as Organic Sensitizers for Highly Efficient Dye-Sensitized Solar Cells. *J. Mater. Chem.* **2012**, *22*, 4040−4049.

DOI: 10.1021/am507503d
ACS Appl. Mater. Interfaces 2015, 7, 1879−1891